

# Improved Pion–Kaon Identification in Heavy-Ion Collisions with a Two-Dimensional Transformation

Shaowei Lan,<sup>1,\*</sup> Bijun Fan,<sup>2,†</sup> and Like Liu<sup>2,‡</sup>

<sup>1</sup>*School of Electrical and Mechanical Engineering,  
Pingdingshan University, 467000 Pingdingshan, China*

<sup>2</sup>*Key Laboratory of Quark & Lepton Physics (MOE) and Institute of Particle Physics,  
Central China Normal University, Wuhan 430079, China*

(Dated: March 5, 2026)

Accurate identification of charged pions and kaons is essential for precision measurements in relativistic heavy-ion collisions, but becomes increasingly challenging at intermediate and high transverse momentum due to the overlap between time-of-flight mass-square ( $m^2$ ) and ionization energy loss ( $n\sigma$ ) distributions. In this work, we present a two-dimensional shift and rotation method that exploits the correlated information between  $m^2$  and  $n\sigma$  to enhance particle identification performance. The method is validated using Au+Au collision events generated with the AMPT model, where detector response effects are incorporated through a data-driven smearing procedure tuned to reproduce the particle identification performance of the STAR experiment. The reconstructed pion and kaon transverse momentum distributions show excellent agreement with the AMPT input, maintaining a purity exceeding 98% at high  $p_T$  and extend the reliable identification range up to  $p_T \approx 3$  GeV/ $c$ . The extracted elliptic flow  $v_2$  remains consistent with the input over the extended  $p_T$  range, demonstrating that the proposed method provides a robust framework for high precision identified hadron measurements.

arXiv:2603.03353v1 [physics.ins-det] 27 Feb 2026

---

\* shaoweilan@pdsu.edu.cn

† bjfan@mails.cnu.edu.cn

‡ likeliu@mails.cnu.edu.cn

## I. INTRODUCTION

Relativistic heavy-ion collisions, such as those conducted at the Relativistic Heavy Ion Collider (RHIC) and the Larger Hadron Collider (LHC), accelerate heavy nuclei to nearly the speed of light and collide them to recreate the extreme energy density and temperature conditions of the early universe. These collisions offer a unique opportunity to study the properties of a novel state of matter known as the quark-gluon plasma (QGP), in which these quarks and gluons are no longer confined within hadrons [1, 2]. The QGP medium is studied indirectly by analyzing the properties of the hadrons produced in the final state of the collisions. A variety of observables including collective flow, hadron yield distributions, and jet quenching patterns have been proposed and extensively studied to probe the transport and collective behavior of the QGP [3–9]. Central to all these measurements is the accurate identification of particle species, as different hadrons carry distinct information about the system’s evolution, freeze-out dynamics, and the underlying QCD processes.

Among the hadrons commonly observed, charged pions ( $\pi^\pm$ ), kaons ( $K^\pm$ ), and protons ( $p/\bar{p}$ ) are of particular importance due to their relatively long lifetimes and stable decay properties. These particles can be directly detected and identified on a track-by-track basis using detectors such as Time Projection Chamber (TPC) [10] and Time-of-Flight (TOF) systems [11]. The TPC provides measurements of the ionization energy loss ( $dE/dx$ ), while the TOF system offers timing information that can be used to calculate the squared mass ( $m^2$ ) of the particle. Together, these detectors enable particle identification (PID) in a wide range of transverse momentum ( $p_T$ ) [12], although with increasing difficulty at high  $p_T$  where the resolution of PID signals overlaps between species. In contrast, hadrons originating from the decay of short-lived resonances or strange baryons, such as  $\Lambda$ ,  $\Xi$ , or  $K_S^0$ , have lifetimes too short to be directly measured. These particles are typically reconstructed through their weak decay topologies using secondary vertex identification techniques, which are sensitive to tracking resolution and background contamination. These particle reconstruction is performed using the KF Particle Finder package based on the Kalman Filter method [13]. A persistent challenge in hadron identification lies in the separation of pions and kaons at intermediate to high  $p_T$  (typically above 2.0 GeV/c). Due to their same electric charge and relatively small mass difference [14], the conventional methods, based on one-dimensional fits to  $dE/dx$  or  $m^2$  distributions [15], often suffer from overlap in these momentum regions, leading to reduced purity and increased systematic uncertainty in physics analyses. The purity of identified particle samples is critically important for the extraction of physics observables. For instance, inaccuracies in pion and kaon separation can lead to biases in the measurement of collective flow coefficients, particle spectra, and correlation functions. Improving PID performance, especially in the high momentum regime, is a key objective in ongoing and future heavy-ion collision experiments [16–18].

In this study, a data-driven, two-dimensional shift and rotation method for enhancing pion and kaon separation at high  $p_T$  is introduced. This approach, originally inspired by techniques employed in the STAR collaboration [19–23], utilizing both the  $n\sigma$  (normalized  $dE/dx$ ) [24] from the TPC and the  $m^2$  from the TOF detector. By redefining the coordinate system through an optimal transformation, the method simultaneously exploits the PID information from both detectors to construct a new variable space where pions and kaons are more clearly [20, 23].

This paper is organized as follows. Section II introduces the AMPT model and the data-driven detector smearing procedure used to emulate realistic experimental particle identification performance. The proposed two-dimensional shift and rotation method for optimizing particle separation in the combined  $n\sigma$ – $m^2$  space is then described in detail. Section III presents a systematic evaluation of the method performance through comparisons between the extracted pion and kaon yields and the corresponding AMPT input, and discusses the extraction of elliptic flow coefficients ( $v_2$ ) using the two-dimensional approach. Finally, a summary is given in Section IV.

## II. METHOD

This simulation is performed using a multi-phase transport model (AMPT) [25] to generate Au+Au collision events at  $\sqrt{s_{NN}} = 200$  GeV. In this study, the string melting version of AMPT [26] is employed, which includes four main components: fluctuating initial conditions from HIJING, partonic scatterings described by the Zhang’s Parton Cascade (ZPC), hadronization via a quark coalescence mechanism, and subsequent hadronic interactions modeled by the ART framework. The AMPT model has been extensively validated against experimental measurements at RHIC and LHC energies and has demonstrated its capability to reproduce a wide range of observables, including particle spectra and anisotropic flow coefficients [27–29].

In the AMPT model, detector resolution effects are not included, particle masses are fixed to their true values, and no  $n\sigma$  information is provided. As a result, particle identification in the model is ideal and free from detector-related limitations. To simulate realistic experimental conditions, where particle identification is limited by finite detector resolution, a data-driven smearing procedure is applied to the  $m^2$  and  $n\sigma$  distribution of charged pions and kaons.

Inspired by the particle identification performance observed in the STAR experiment [5], smearing parameterizations for the mean values and widths ( $\sigma$ ) of the  $m^2$  and  $n\sigma_\pi$  distributions as a function of transverse momentum are

constructed and shown in Fig. 1. These parameterized curves exhibit a clear  $p_T$  dependence, reflecting the gradual degradation of detector particle identification resolution at higher transverse momentum, a behavior that is qualitatively similar across different collision energies. The resulting parameterizations are applied to the AMPT model output to smear the  $m^2$  and  $n\sigma$  values of charged pions and kaons on a track-by-track basis. This procedure introduces realistic,  $p_T$ -dependent PID resolution effects into the model while preserving the intrinsic event-by-event correlations and anisotropic flow signals. The smeared AMPT sample thus provides a consistent and controlled framework for evaluating the performance of the proposed two-dimensional particle identification method.

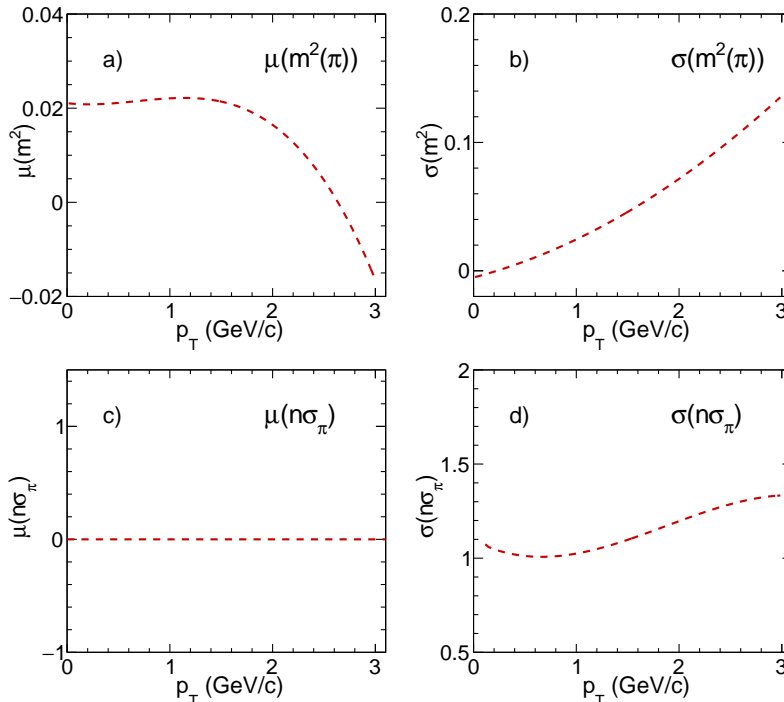


FIG. 1. Transverse momentum ( $p_T$ ) dependence of the smearing parameters used to model the detector response in the particle identification variables: (a) mean of the time-of-flight mass-squared ( $m^2$ ), (b) width ( $\sigma$ ) of the  $m^2$  distribution, (c) mean of  $n\sigma_\pi$ , and (d) width ( $\sigma$ ) of the  $n\sigma_\pi$  distribution.

The left panels of Fig. 2 show the two-dimensional distributions of  $m^2$  versus  $n\sigma_\pi$  in the transverse momentum intervals  $2.0 < p_T < 2.2$  GeV/c (top) and  $2.8 < p_T < 3.0$  GeV/c (bottom). These distributions clearly illustrate the increasing overlap between pion and kaon bands with increasing  $p_T$ . In the conventional particle identification procedure commonly employed in STAR analyses, an initial selection is applied using the  $n\sigma_\pi$  variable, typically requiring  $|n\sigma_\pi| < 3$ , to enhance pion purity. Within each  $p_T$  interval, a one-dimensional  $m^2$  distribution is then constructed from the selected tracks, as shown by the black solid circles in Fig. 3, and fitted with a sum of Gaussian functions, with each component corresponding to a different particle species. Particle yields are subsequently extracted by integrating the fitted function within a window defined by the mean  $\pm 3\sigma$  of each peak. Fig. 3 presents a representative example of this conventional approach for pion and kaon identification in the  $p_T$  range of 2.4-2.6 GeV/c. While this method performs adequately at low transverse momentum, it begins to exhibit pronounced limitations in the intermediate  $p_T$  region. In particular, the kaon peak becomes strongly overlapped with the dominant pion distribution and is no longer clearly separable. At higher transverse momentum ( $p_T \gtrsim 2.6$  GeV/c), the kaon signal is effectively buried under the pion background, making reliable particle identification increasingly difficult and ultimately infeasible within this one-dimensional framework.

To improve the particle identification performance, a two-dimensional shift and rotation transformation is applied to the  $m^2$  versus  $n\sigma_\pi$  distribution, as illustrated in the right panels of Fig. 2. This procedure defines a new coordinate system,  $x(n\sigma_\pi, m^2)$  and  $y(n\sigma_\pi, m^2)$ , obtained through a linear shift and rotation followed by a translation of the original variables. The transformation parameters are optimized such that the effective Gaussian widths of the particle peaks along  $x$  and  $y$  directions become comparable, while the pion and kaon distributions are predominantly aligned along the  $x$  axis. This redefinition of the variable space maximizes the separation between particle species and facilitates a more robust and stable particle identification.

The transformation procedure consists of three sequential steps – scaling, shifting, and rotation – and is mathematically defined by Eqs. 1,2,3,4,5.

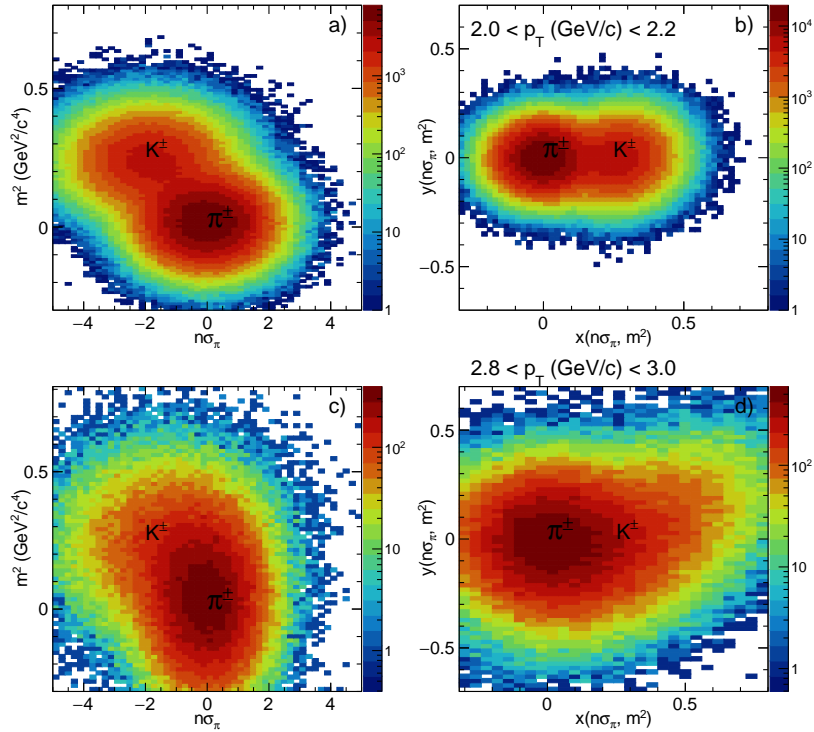


FIG. 2. Two-dimensional particle identification distributions for charged pions and kaons before and after applying the shift and rotation transformation. Panels (a) and (c) show the raw  $m^2$  versus  $n\sigma_\pi$  distributions in the transverse momentum intervals  $2.0 < p_T < 2.2$  and  $2.8 < p_T < 3.0$  GeV/c, respectively. Panels (b) and (d) present the corresponding distributions in the transformed coordinate system  $(x, y)$  after the two-dimensional shift and rotation, for the same  $p_T$  intervals.

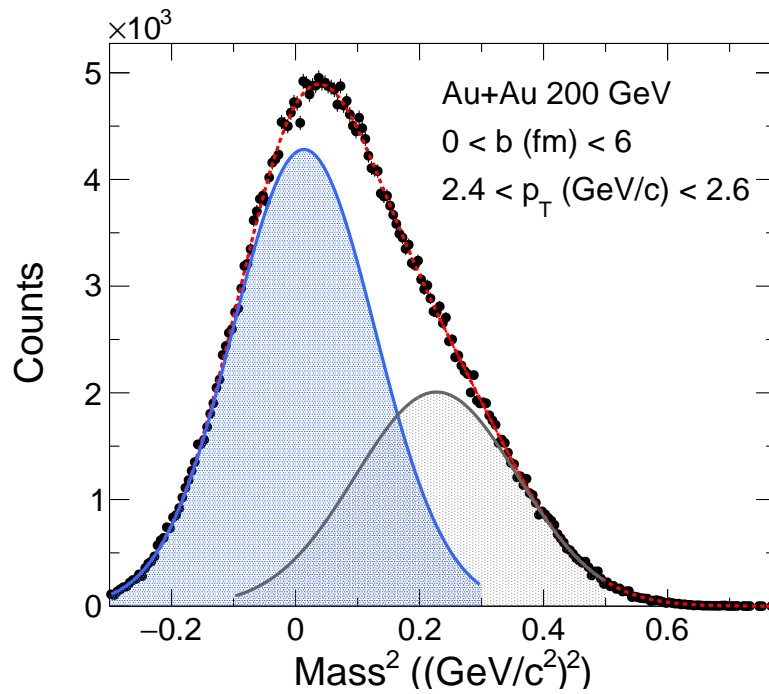


FIG. 3. Simulated  $m^2$  distribution of charged particles in the transverse momentum interval  $2.4 < p_T < 2.6$  GeV/c. The red dashed line represents the multi-Gaussian fit to the inclusive  $m^2$  distribution, while the blue and gray solid lines indicate the pion and kaon components extracted from the fit, respectively.

First, a scale factor  $f_{\text{scale}}$  is introduced to normalize the widths of the distributions along the  $n\sigma_\pi$  and  $m^2$  axes. The scaling step equalizes the effective resolution of the two variables, ensuring that neither dimension dominates the particle separation in the transformed space. Next, a linear translation is applied to shift the centroid of the pion distribution to the origin of the coordinate system. The shift parameter,  $\mu(n\sigma_\pi)$  and  $\mu(m^2(\pi))$ , correspond to the mean values of the pion  $n\sigma_\pi$  and  $m^2$  distributions, respectively. These parameters are taken obtained from the parameterized  $p_T$ -dependent functions shown in Fig. 1. Following the scaling and shifting steps, a rotation is applied to further optimize the alignment of the particle bands. The rotation angle  $\alpha$  is determined from the relative orientation of the kaon band with respect to the pion band in the two-dimensional  $m^2-n\sigma_\pi$  space. A counterclockwise rotation by angle  $\alpha$  is then performed, such that the kaon band becomes aligned parallel to the pion band along the  $x$  axis.

As a result of these transformations, the pion and kaon distributions from two well-separated and horizontally aligned peaks in the transformed coordinate system. Since the transformation is linear and applied uniformly on a track-by-track basis, it preserves event-by-event correlations and does not introduce artificial azimuthal modulations, making it suitable for subsequent yield and flow analyses.

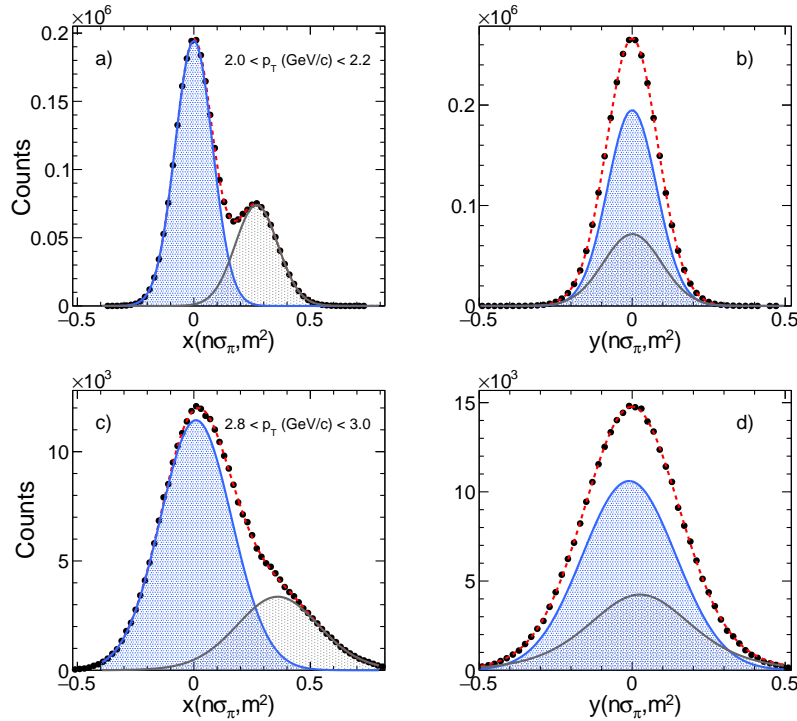


FIG. 4. Projections of the transformed two-dimensional distributions for charged pions and kaons. (a) and (b) Projections onto the new  $x$  and  $y$  axes, respectively, for  $2.0 < p_T < 2.2$  GeV/c. (c) and (d) Corresponding projections for  $2.8 < p_T < 3.0$  GeV/c. The red dashed curves denote multi-Student- $t$  fits, while the blue and gray solid lines represent the pion and kaon components.

$$f_{\text{scale}} = \sigma(n\sigma_\pi)/\sigma(m^2(\pi)) \quad (1)$$

$$x' = (n\sigma_\pi - \mu(n\sigma_\pi))/f_{\text{scale}} \quad (2)$$

$$y' = m^2 - \mu(m^2(\pi)) \quad (3)$$

$$\alpha = -\tan^{-1} \left[ \frac{\mu(m^2(K)) - \mu(m^2(\pi))}{(\mu(n\sigma_K) - \mu(n\sigma_\pi))/f_{\text{scale}}} \right] \quad (4)$$

$$\begin{pmatrix} x(n\sigma_\pi, m^2) \\ y(n\sigma_\pi, m^2) \end{pmatrix} = \begin{pmatrix} \cos(\alpha) & -\sin(\alpha) \\ \sin(\alpha) & \cos(\alpha) \end{pmatrix} \begin{pmatrix} x' \\ y' \end{pmatrix} \quad (5)$$

As shown in the right panels of Fig. 4, the transformation leads to two notable improvements in the particle distributions. First, for each particle species, the widths of the distributions along the  $x$  and  $y$  axes become approximately identical. Second, the pion and kaon distributions are well aligned along the horizontal axis in the transformed coordinate system. These features provide clear advantages for particle identification. The approximate symmetry of the particle distributions along both axes enables a simplified and more robust fitting strategy in the transformed space. In particular, the particle distributions are described using a two-dimensional Student's  $t$  function in the  $x$ - $y$  plane. Owing to the comparable widths along the two axes, the number of free fit parameters is effectively reduced, which significantly improves the stability and convergence of the fitting procedure.

Furthermore, the horizontal alignment of the pion and kaon maximizes the separation between the two particle species in the transformed space. The enhanced separation substantially reduces the overlap between pion and kaon distributions, thereby suppressing cross-contamination in the extracted yields and leading to improved particle identification performance.

In this analysis, the two-dimensional distributions of individual particle species are modeled using a two-dimensional Student's  $t$  function, as defined in Eq. 6. Compared to a standard Gaussian function, the Student's  $t$  function includes an additional degree-of-freedom parameter,  $\nu$ , which provides enhanced flexibility in describing non-Gaussian tails that are commonly observed in experimental particle identification distribution. Such deviations from Gaussian behavior can originate from finite detector resolution effects as well as from underlying physics processes in relativistic heavy-ion collisions. Consequently, relative to Gaussian-based parameterizations adopted in earlier STAR analyses, the Student's  $t$  function offers a more accurate and stable description of the data.

The one-dimensional Student's  $t$  function is characterized by three parameters: the mean( $\mu$ ), the width( $\sigma$ ), and the degree of freedom( $\nu$ ). When extended to two dimensions, an additional normalization parameter is introduced for each particle species, as summarized in Eq. 7. To further limit the number of independent fit parameters and avoid over-parameterization, the widths of kaon distributions are constrained using empirically determined relationships with the pion and proton widths. This strategy maintains physical consistency across different particle species while improving the robustness of the fit.

In total, the combined two-dimensional multi-particle fit function describing the pion and kaon distributions contains 13 free parameters, as listed in Eq. 8. Given the relatively large parameter space and potential correlations among parameters, the fitting procedure is performed iteratively. An initial fit is first used to obtain reasonable starting values, which are then refined through successive iterations until convergence is achieved. This iterative approach ensures a stable and physically meaningful solution, particularly in kinematic regions with limited statistical precision.

$$f_{x(y)} = \frac{\Gamma\left(\frac{\nu_{x(y)}+1}{2}\right)}{\Gamma\left(\frac{\nu_{x(y)}}{2}\right)\sqrt{\pi\nu_{x(y)}\sigma_{x(y)}^2}} \left[1 + \frac{1}{\nu_{x(y)}} \left(\frac{x(y)-\mu_{x(y)}}{\sigma_{x(y)}}\right)^2\right]^{-\frac{\nu_{x(y)}+1}{2}} \quad (6)$$

$$f_{particle} = N_0 \times f_{x,particle} \times f_{y,particle} \quad (7)$$

$$f_{fit} = f_{\pi} + f_K \quad (8)$$

After applying the transformation described above, the yields of charged pions and kaons are extracted by projecting the two-dimensional distribution onto the  $x$  axis. As shown in the left panels of Fig. 4, the resulting one-dimensional distributions are well described by the multi-component Student's  $t$  function used in the fit. The pion and kaon peaks are clearly separated, enabling a stable and reliable extraction of particle yields over the full transverse momentum range considered. For each transverse momentum ( $p_T$ ) interval, particle yields are obtained by integrating the fitted function within a  $\pm 3\sigma$  window centered around the corresponding particle peak.

The right panels of Fig. 4 show the projection of the same two-dimensional distribution onto the  $Y$  axis. The resulting distributions are narrow and approximately symmetric, indicating that, after the shift and rotation, both pion and kaon distributions are effectively aligned along the horizontal direction in the transformed coordinate system. This behavior confirms the effectiveness of the shift and rotation procedure in optimizing the particle separation. The improved alignment, together with the reduced effective parameter complexity in the  $X$ - $Y$  space, enhances both the robustness of the fitting procedure and the reliability of the extracted particle yield.

### III. RESULTS AND DISCUSSIONS

The top panels of Fig. 5 present the transverse momentum ( $p_T$ ) dependence of the extracted yields for charged pions and kaons obtained using the proposed two-dimensional shift and rotation method. The results are directly compared

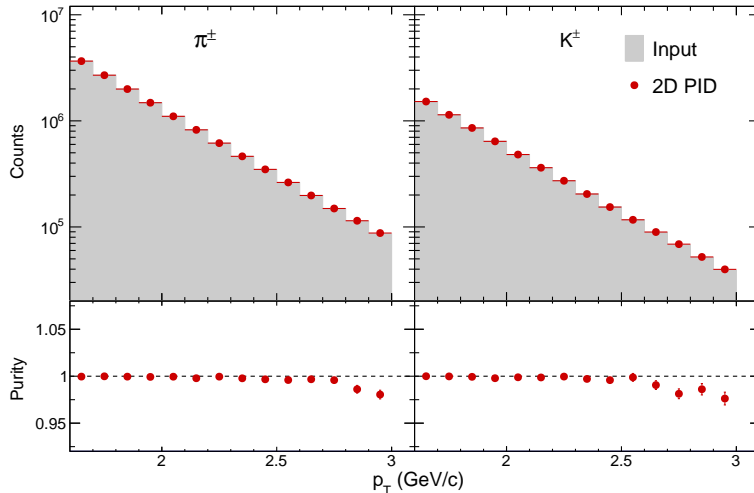


FIG. 5. Transverse momentum ( $p_T$ ) distribution of charged pions and kaons from the AMPT input (gray bands) and the two-dimensional PID extraction (red solid circles). The lower panels present the corresponding PID purity versus  $p_T$ .

to the corresponding true input yields from the AMPT model. The red solid circles denote the yields extracted with the two-dimensional method, while the gray shadow represent the AMPT input. Over the full transverse momentum range considered, the extracted yields show excellent agreement with the model input. In particular, even in the high- $p_T$  region up to  $p_T = 3.0$  GeV/ $c$ , where particle identification becomes increasingly challenging due to reduced detector resolution, the two-dimensional method reproduces the input yields with a deviation of less than 2% for both pions and kaons. This demonstrates the robustness of the method against deteriorating particle separation at high transverse momentum.

The bottom panels of Fig. 5 show the extraction purity, defined as the ratio of the extracted yield to the AMPT input yield. The purity remains close to unity across the entire  $p_T$  range, indicating a particle identification purity exceeding 98% even at the highest transverse momenta. The stability of the extracted yields is further confirmed by varying fitting range and integration window, with consistent results observed within statistical uncertainties. The ability of the method to maintain high purity and accurate yield extraction up to  $p_T = 3.0$  GeV/ $c$  represents a significant extension of the effective particle identification reach. This enhanced high- $p_T$  capability is essential for precision measurements that rely on identified hadrons, particularly for observables with strong transverse momentum dependence, such as anisotropic flow and number-of-constituent-quark scaling studies.

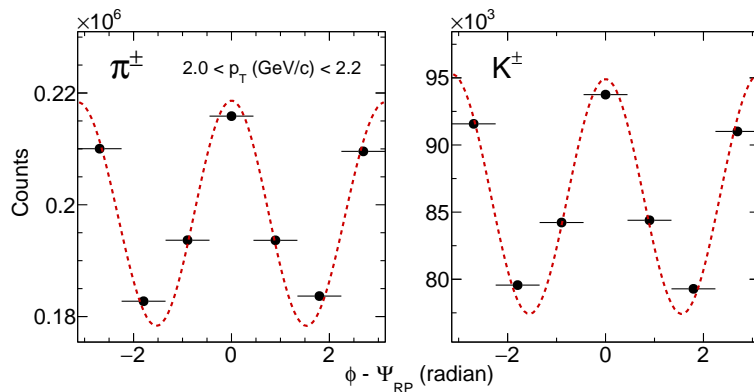


FIG. 6. Azimuthal ( $\phi - \Psi_{RP}$ ) distributions of charged pions (left) and kaons (right) in the transverse momentum range  $2.0 < p_T < 2.2$  GeV/ $c$ . The black solid circles represent the yields obtained using the two-dimensional PID method, while the red dashed lines show the corresponding fits used to extract the elliptic flow coefficient  $v_2$ .

To further validate the performance of the proposed two-dimensional particle identification method, its impact on anisotropic flow measurements by extracting the elliptic flow coefficient  $v_2$  for charged pions and kaons. The analysis is performed using the event plane method [30, 31], and the extracted results are directly compared with the known

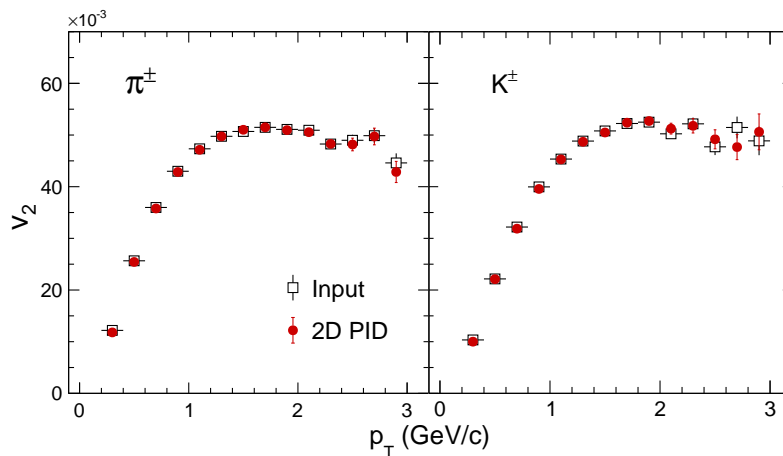


FIG. 7. Transverse momentum ( $p_T$ ) dependence of the elliptic flow  $v_2$  for charged pions (left) and kaons (right). The black open squares represent the AMPT input, while the red solid circles show the results extracted using the two-dimensional PID method.

input values from the AMPT model. In the AMPT simulation, the true event geometry is explicitly available, allowing the input elliptic flow to be calculated with respect to the reaction plane according to  $v_2 = \langle \cos[2(\phi - \Psi_{\text{RP}})] \rangle$ , where  $\phi$  is the azimuthal angle of the particle and  $\Psi_{\text{RP}}$  denotes the reaction plane angle. The average is taken over all particles in all events. In the present setup, the reaction plane is fixed at  $\Psi_{\text{RP}} = 0$ , which simplifies the evaluation of the input  $v_2$ .

To extract  $v_2$  from reconstructed particle yields, the two-dimensional shift and rotation method is applied on a track-by-track basis. For each transverse momentum ( $p_T$ ) interval, the azimuthal angle relative to the reaction plane,  $\phi - \Psi_{\text{RP}}$ , is divided into seven uniform bins. Within each bin, pion and kaon yields are independently reconstructed using the two-dimensional particle identification technique, resulting in yield distribution as a function of  $\phi - \Psi_{\text{RP}}$  for each  $p_T$  interval. The azimuthal yield distribution are fitted with the following Fourier expansion:

$$\frac{dN}{d(\phi - \Psi_{\text{RP}})} \propto N_0 [1 + 2v_1 \cos(\phi - \Psi_{\text{RP}}) + 2v_2 \cos(2(\phi - \Psi_{\text{RP}}))] \quad (9)$$

where the  $v_1$  and  $v_2$  represent the first two harmonic flow coefficients. Contributions from higher-order harmonics are expected to be negligible within the statistical precision of the present study and are therefore not included in the fit.

Figure 6 shows representative examples of the azimuthal yield distributions and the corresponding fits for pions and kaons in the transverse momentum interval 2.0–2.2 GeV/c. The extracted  $v_2$  values as a function of  $p_T$  are summarized in Fig. 7, together with the AMPT input results. Within statistical uncertainties, the  $v_2$  values obtained using the two-dimensional particle identification method are in good agreement with the AMPT input over the entire  $p_T$  range for both pions and kaons.

Although the overall magnitude of  $v_2$  is relatively insensitive to moderate particle identification uncertainties, the improved particle separation achieved by the two-dimensional shift and rotation method provides enhanced robustness, particularly at higher transverse momentum where species overlap becomes increasingly severe. This feature is crucial for precision flow measurements and for differential studies that rely on identified hadrons in the intermediate and high  $p_T$  region.

#### IV. SUMMARY

In summary, we present a data-driven particle identification method based on a two-dimensional shift and rotation transformation that exploits the correlated information of  $m^2$  and  $n\sigma_\pi$ . The performance of the proposed technique is evaluated using simulated Au+Au collisions generated with the AMPT model. By construction, the method preserves event-by-event correlations and is therefore suitable for anisotropic flow analyses. Comparisons with the known AMPT input demonstrate that the extracted pion and kaon yields obtained with the two-dimensional method remain in excellent agreement with the input over the entire studied transverse momentum range. In particular, the proposed approach significantly extends the effective particle identification capability to higher transverse momentum. While conventional one-dimensional techniques become ineffective about  $p_T \approx 2.4$ – $2.6$  GeV/c, the two-dimensional

method maintains a yield purity exceeding 98% up to  $p_T = 3.0$  GeV/ $c$ . This extended kinematic reach represents a substantial improvement in PID performance and enables reliable measurements in a momentum region that is traditionally inaccessible for identified hadrons.

The impact of the improved particle identification on elliptic flow measurements is further examined by extracting  $v_2$  via azimuthal yield fits. The reconstructed  $v_2$  values for both pions and kaons are consistent with the AMPT input within statistical uncertainties, confirming that the proposed method does not introduce biases in flow observables. The extended  $p_T$  reach provided by this technique is particularly relevant for studies of identified-hadron flow and number-of-constituent-quark scaling, which rely critically on precise measurements at intermediate and high transverse momentum. Overall, the two-dimensional shift and rotation method offers a robust and general framework for improving PID performance in future high-precision heavy-ion measurements.

The proposed method has broad applicability and can be adapted to future experiments such as the Cooling Storage Ring External-target Experiment (CEE) at HIRFL/HIAF, the Nuclotron-based Ion Collider Facility (NICA) at JINR, and the Compressed Baryonic Matter (CBM) experiment at FAIR [32–38]. These facilities will explore different regions of the QCD phase diagram with varying collision energies and system sizes, where precise particle identification across extended transverse momentum ranges will be crucial. The two-dimensional shift and rotation approach provides a flexible framework that can be tuned to the specific detector characteristics and PID requirements of these experiments, thereby enhancing their capability to extract clean signals of identified hadrons for studying the properties of dense nuclear matter.

## ACKNOWLEDGMENTS

We thank Prof. Shusu Shi for useful discussions. This work was supported by the Doctoral Scientific Research Foundation of Pingdingshan University (PXY-BSQD-2023016), the Natural Science Foundation of Henan under contract No. 252300420921, the National Key Research and Development Program of China under Contract Nos. 2024YFA1610700.

- 
- [1] P. Braun-Munzinger and J. Stachel, *Nature* **448**, 302 (2007).
  - [2] E. V. Shuryak, *Phys. Lett. B* **78**, 150 (1978).
  - [3] M. Gyulassy and M. Plumer, *Phys. Lett. B* **243**, 432 (1990).
  - [4] G.-Y. Qin and X.-N. Wang, *Int. J. Mod. Phys. E* **24**, 1530014 (2015), arXiv:1511.00790 [hep-ph].
  - [5] L. Adamczyk *et al.* (STAR), *Phys. Rev. Lett.* **116**, 062301 (2016), arXiv:1507.05247 [nucl-ex].
  - [6] L. Adamczyk *et al.* (STAR), *Phys. Rev. C* **96**, 044904 (2017), arXiv:1701.07065 [nucl-ex].
  - [7] J. Chen *et al.*, *Nucl. Sci. Tech.* **35**, 214 (2024), arXiv:2407.02935 [nucl-ex].
  - [8] X. Luo, S. Shi, N. Xu, and Y. Zhang, *Particles* **3**, 278 (2020), arXiv:2004.00789 [nucl-ex].
  - [9] A. Bzdak *et al.*, *Phys. Rept.* **853**, 1 (2020).
  - [10] M. Anderson *et al.*, *Nucl. Instrum. Meth. A* **499**, 659 (2003).
  - [11] F. Geurts *et al.*, *Nucl. Instrum. Meth. A* **533**, 60 (2004).
  - [12] K. H. Ackermann *et al.* (STAR), *Nucl. Instrum. Meth. A* **499**, 624 (2003).
  - [13] I. Kisel (CBM), *J. Phys. Conf. Ser.* **1070**, 012015 (2018).
  - [14] M. Aguilar-Benitez *et al.*, *Z. Phys. C* **50**, 405 (1991).
  - [15] B. I. Abelev *et al.* (STAR), *Phys. Rev. C* **79**, 034909 (2009), arXiv:0808.2041 [nucl-ex].
  - [16] J. C. Yang *et al.*, *Nucl. Instrum. Meth. B* **317**, 263 (2013).
  - [17] T. Ablyazimov *et al.* (CBM), *Eur. Phys. J. A* **53**, 60 (2017), arXiv:1607.01487 [nucl-ex].
  - [18] V. Kekelidze, A. Kovalenko, R. Lednický, V. Matveev, I. Meshkov, A. Sorin, and G. Trubnikov, *Nucl. Phys. A* **956**, 846 (2016).
  - [19] L. Adamczyk *et al.* (STAR), *Phys. Rev. Lett.* **110**, 142301 (2013), arXiv:1301.2347 [nucl-ex].
  - [20] L. Adamczyk *et al.* (STAR), *Phys. Rev. C* **88**, 014902 (2013), arXiv:1301.2348 [nucl-ex].
  - [21] L. Adamczyk *et al.* (STAR), *Phys. Rev. C* **93**, 014907 (2016), arXiv:1509.08397 [nucl-ex].
  - [22] L. Adamczyk *et al.* (STAR), *Phys. Rev. C* **86**, 054908 (2012), arXiv:1206.5528 [nucl-ex].
  - [23] M. S. Abdallah *et al.* (STAR), *Phys. Lett. B* **827**, 137003 (2022), arXiv:2108.00908 [nucl-ex].
  - [24] H. Bichsel, *Nucl. Instrum. Meth. A* **562**, 154 (2006).
  - [25] Z.-W. Lin, C. M. Ko, B.-A. Li, B. Zhang, and S. Pal, *Phys. Rev. C* **72**, 064901 (2005), arXiv:nucl-th/0411110.
  - [26] Z.-w. Lin and C. M. Ko, *Phys. Rev. C* **65**, 034904 (2002), arXiv:nucl-th/0108039.
  - [27] Z.-W. Lin, *Phys. Rev. C* **90**, 014904 (2014), arXiv:1403.6321 [nucl-th].
  - [28] S. Lan, Z.-W. Lin, S. Shi, and X. Sun, *Phys. Lett. B* **780**, 319 (2018), arXiv:1710.03895 [nucl-th].
  - [29] L.-K. Liu and S. Shi, *Phys. Rev. C* **112**, 064912 (2025), arXiv:2508.21577 [nucl-th].
  - [30] S. A. Voloshin, A. M. Poskanzer, and R. Snellings, *Landolt-Bornstein* **23**, 293 (2010), arXiv:0809.2949 [nucl-ex].
  - [31] A. M. Poskanzer and S. A. Voloshin, *Phys. Rev. C* **58**, 1671 (1998), arXiv:nucl-ex/9805001.

- [32] L. Lü, H. Yi, Z. Xiao, M. Shao, S. Zhang, G. Xiao, and N. Xu, *Sci. China Phys. Mech. Astron.* **60**, 012021 (2017).
- [33] L.-K. Liu, H. Pei, Y.-P. Wang, Y. Wang, B. Zhang, N. Xu, and S.-S. Shi, *Nucl. Sci. Tech.* **34**, 100 (2023), arXiv:2302.11759 [nucl-ex].
- [34] B. Zhang, L.-K. Liu, H. Pei, S.-S. Shi, N. Xu, and Y. Wang, *Nucl. Sci. Tech.* **34**, 176 (2023), arXiv:2304.14411 [physics.ins-det].
- [35] W. Wu, X. He, Y. Ren, D. Shen, S. Shi, and X. Sun, (2025), arXiv:2503.22774 [physics.ins-det].
- [36] A. Kisiel (MPD), *J. Phys. Conf. Ser.* **1602**, 012021 (2020).
- [37] R. Abdulin *et al.* (MPD), *Rev. Mex. Fis.* **71**, 041201 (2025), arXiv:2503.21117 [nucl-ex].
- [38] A. Agarwal *et al.* (CBM), *Nucl. Instrum. Meth. A* **1082**, 171059 (2026), arXiv:2505.20517 [physics.ins-det].